Journal of Controlled Release 297 (2019) 39–47

Contents lists available at ScienceDirect

Journal of Controlled Release

journal homepage: www.elsevier.com/locate/jconrel

Pharmacokinetics and pharmacodynamics of liposomal chemophototherapy with short drug-light intervals

Dandan Luo[a], Kevin A. Carter[a], Emilie A.G. Molins[b], Ninfa L. Straubinger[b], Jumin Geng[a], Shuai Shao[a], William J. Jusko[b], Robert M. Straubinger[b], Jonathan F. Lovell[a,*]

[a] Department of Biomedical Engineering, University at Buffalo, State University of New York, Buffalo, NY 14260, USA
[b] Department of Pharmaceutical Sciences, University at Buffalo, State University of New York, Buffalo, NY 14214, USA

ARTICLE INFO

Keywords:
PoP liposomes
Chemophototherapy
Pharmacokinetics
Pharmacodynamics
Photodynamic therapy
Drug delivery

ABSTRACT

Chemophototherapy (CPT) merges photodynamic therapy with chemotherapy and can substantially enhance drug delivery. Using a singular liposomal formulation for CPT, we describe a semi-mechanistic pharmacokinetic-pharmacodynamic (PK/PD) model to investigate observed antitumor effects. Long-circulating, sterically-stabilized liposomes loaded with doxorubicin (Dox) stably incorporate small amounts of a porphyrin-phospholipid (PoP) photosensitizer in the bilayer. These were administered intravenously to mice bearing low-passage, patient-derived pancreatic cancer xenografts (PDX). Dox PK was described with a two-compartment model and tumor drug disposition kinetics were modeled with first-order influx and efflux rates. Tumor irradiation with 665 nm laser light (200 J/cm^2) 1 h after liposome administration increased tumor vascular permeabilization and drug accumulation, which was accounted for in the PK/PD model with increased tumor influx and efflux rates by approximately 12- and 4- fold, respectively. This modeling approach provided an overall 7-fold increase in Dox area under the curve in the tumor, matching experimental data (7.4-fold). A signal transduction model based on nonlinear direct cell killing accounted for observed tumor growth patterns. This PK/PD model adequately describes the CPT anti-PDX tumor response based on enhanced drug delivery at the short drug-light interval used.

1. Introduction

Late-stage pancreatic cancer is typically a lethal disease with poor treatment options [1,2]. Insufficient drug delivery to tumor sites is often a major contributing factor for the poor survival. Pancreatic ductal adenocarcinoma (PDAC) is characterized by low vascular density, perfusion, and permeability as well as amplification of tumor associated stromal tissue (desmoplasia), which together prevent sufficient delivery of chemotherapeutics [3]. Enzymatic degradation of hyaluronan, a major component of stroma, is a promising approach for enhancing drug delivery in PDAC [4] and approaches that reduce hyaluronan density have been shown to enhance liposomal delivery to tumor models [5,6]. Depletion of tumor stromal tissue by inhibition of sonic hedgehog cellular signaling pathway can increase tumor microvessel density and perfusion and enhance delivery of chemotherapeutics and nanotherapeutics [7,8].

Long circulating liposomal chemotherapy can be an effective tumor treatment compared to the free drug [9]. Liposomal irinotecan has recently been approved as a second-line treatment in late-stage pancreatic cancer after favorable phase III trials results in which it was combined with fluorouracil and folinic acid [10,11]. Prior clinical studies in pancreatic cancer with long-circulating liposomal doxorubicin (DOXIL) did not show objective responses when used as a monotherapy [12]. To improve outcomes, numerous approaches have aimed to improve liposomal drug delivery including targeting [13,14], microenvironment-triggered drug release [15], and external stimuli-enhanced delivery [16].

Chemophototherapy (CPT) incorporates two cancer therapy modalities: chemotherapy and phototherapy [17]. Photodynamic therapy has been approved to treat several tumor types [18]. When photosensitizers are circulating in the blood, photodynamic therapy (PDT) is able to permeabilize tumor vasculature and enhance delivery of nanotherapeutics, likely by damaging tumor endothelial cells and augmenting endothelial intercellular gaps [19–21]. By stably incorporating a small amount of porphyrin-phospholipid (PoP) into the bilayer of liposomes, we developed photoactivatable doxorubicin (Dox) encapsulated in PoP liposomes that can be triggered by near infrared light (NIR) and deliver actively-loaded [22–24] or passively-loaded [25] drugs into irradiated tumors. We previously established a long-circulating formulation of Dox in PoP liposomes (termed LC-Dox-PoP) that

* Corresponding author.
E-mail address: jflovell@buffalo.edu (J.F. Lovell).

https://doi.org/10.1016/j.jconrel.2019.01.030
Received 21 May 2018; Received in revised form 18 November 2018; Accepted 22 January 2019
Available online 23 January 2019

includes 2 mol% PoP in a DOXIL-like liposome formulation [26]. This work uses the same LC-Dox-PoP formulation. As light has limited tissue penetration, our proposed treatment with LC-Dox-PoP liposomes with laser treatment could be carried out relatively non-invasively using optical fibers that are inserted into large or deep tumors.

Several nanoparticle- and host-related factors impact liposome pharmacokinetics and pharmacodynamics (PK/PD) [27]. PK/PD models of sterically-stabilized Dox liposomes have been reported previously [28], and heat-triggered liposomal Dox release from thermosensitive liposomes has been modeled [29]. However, tumor PK and PK/PD modeling of LC-Dox-PoP liposomes, or other single-agent CPT systems, have not been explored yet.

We assessed LC-Dox-PoP liposomes in a patient-derived xenograft (PDX) PDAC model heterozygous for the G12D KRAS mutation (Fig. S1) and that recapitulates the tumor drug delivery barriers in pancreatic cancer. PDX models are valuable tools for assessing cancer therapeutics [30]. We develop a semi-mechanistic PK/PD model for quantitative analysis of observed PDT-induced vascular permeabilization and the resulting improvement in anti-tumor efficacy.

2. Materials and methods

2.1. Liposome preparation

1,2-distearoyl-sn-glycero-3-phosphocholine (DSPC; # LP-R4–076), cholesterol (CHOL; # CH-0355), 1,2-Distearoyl-phosphatidylethanolamine-methyl-polyethyleneglycol conjugate-2000 (PEG-lipid; # LP-R4–039) were ordered from Corden Pharma. NVP-LDE225 (Sonidegib) was from Chemietek. The porphyrin-phospholipid (PoP) used was sn-1-palmitoyl, sn-2-pyropheophorbide phosphatidylcholine and was synthesized as previously reported [22]. PoP liposomes [DSPC:PoP:-CHOL:PEG-lipid; 53:2:40:5 mol%] were prepared by a modified hot ethanol injection method followed by high pressure extrusion, as previously described [31]. To generate 10 mL PoP liposomes (20 mg/mL total lipids), lipids were first fully dissolved in 2 mL of hot ethanol, followed by direct injection into 8 mL of 250 mM ammonium sulfate (pH 5.5) buffer at 60 °C. The lipid solution was then passed 10 times at 60 °C through sequentially stacked polycarbonate membranes of 0.2, 0.1, and 0.08 μm pore size using a 10 mL LIPEX nitrogen pressurized extruder (Northern Lipids). Liposomes were then dialyzed with buffer containing 10% sucrose and 10 mM histidine (pH 6.5) to remove free ammonium sulfate. Dox (LC Labs #D-4000) was actively loaded into liposomes via the ammonium sulfate gradient [32] by adding 20 mg/mL Dox solution to the liposomes at a drug to lipid ratio of 1:6 (mol:mol) and incubated at 60 °C for 1 h. Loading efficiency was typically over 95%.

2.2. Tumor model

Animal studies were approved by the Institutional Animal Care and Use Committees of Roswell Park Cancer Institute (RPCI) and the University at Buffalo. Pancreatic adenocarcinoma PDX #18269, was established in SCID mice at RPCI and maintained as described, without dissociation or in vitro culture at any point [33]. Briefly, subcutaneous tumors (passage < 7) were harvested from donor mice, cut into 2 × 2 × 2 mm blocks under cold RPMI-1640 medium, and implanted subcutaneously on the abdominal wall of anesthetized 18 to 20 g C·B-Igh-1^b/IcrTac-Prkdc SCID mice. Treatment was initiated 4 to 6 weeks after implantation, when tumors were ~100 to 300 mm^3. For pharmacokinetic studies, mice were implanted with tumors on the right and left abdominal walls. To probe the KRAS gene of the PDX model, DNA primers were used (forward: 5-GGTGGAGTATTTGATAGTGTATTAACC and reverse: 5-AGAATGGTCCTGCACCAGTAA) to obtain and sequence the human KRAS amplicon, starting with tumor DNA isolated in conventional fashion. The PDX model was found to be heterozygous for the G12D mutation and wildtype for G13 (Fig. S1).

2.3. Pharmacokinetics

SCID mice bearing dual PDX tumors were injected via tail vein with LC-Dox-PoP liposomes at 4 mg/kg Dox (7 groups, $n = 6$ mice per group). One hr post injection, the tumor on one side of the mouse was irradiated (200 mW/cm^2 for 16.7 min, 200 J/cm^2). Mice were sacrificed at 30 min, 4, 10, 24, 48, 72, and 120 h post laser treatment, and blood, tumors, and key organs were collected. Blood was centrifuged at 1500 *g* for 15 min. Serum was collected in capillary tubes (Microvette CB 300Z) and diluted in extraction buffer (0.075 N HCL, 90% isopropanol). Samples were then stored at −20 °C overnight. For analysis, samples were centrifuged at 10,000 *g* for 15 min, and supernatants were collected and analyzed for Dox fluorescence in a 96 well plate reader. Dox concentration was determined fluorometrically from a standard curve [34,35]. Pharmacokinetics of an additional dose, 10 mg/kg LC-Dox-PoP, was also studied in SCID mice bearing PDX for the serum PK model.

To quantify tumor drug uptake, SCID mice bearing PDX tumors were intravenously injected with 4 or 7 mg/kg Dox-loaded PoP liposomes and sacrificed 24 h post injection. Tumors and key organs were collected and washed in PBS. Approx. 100 mg of tissue were weighed and homogenized in 450 μL nuclear lysis buffer [250 mM sucrose, 5 mM Tris-HCl, 1 mM $MgSO_4$, 1 mM $CaCl_2$ (pH 7.6)] with a Bullet Blender Storm homogenizer. Dox was extracted by mixing 900 μL of 0.075 N HCI in 90% isopropanol with 100 μL of homogenate and storing at −20 °C overnight. Samples were then centrifuged at 10,000 *g* for 15 min. The supernatant was collected and the concentrations of Dox (480 nm excitation, 590 nm emission) and PoP (420 nm excitation, 670 nm emission) were determined fluorometrically.

2.4. Fluorescence microscope imaging of drug distribution in tumor

Tumor-bearing SCID mice were administered 10 mg/kg Dox-loaded PoP liposomes intravenously. One hr after intravenous injection, one group of mice was treated with laser for 16.7 min at 200 mW/cm^2 (665 nm, 200 J/cm^2). After 8 h, mice were sacrificed and tumors collected and immediately embedded in OCT embedding compound (VWR #25608–930) in embedding molds, snap frozen in liquid nitrogen and stored at −80 °C prior to use. Tumors were sectioned in a cryostat at −20 °C at 15 μm thickness. Fluorescence microscopy for Dox and PoP was carried out with an EVOS FL Auto microscope with a 20× objective lens. Dox was imaged with filter cubes with 470 nm excitation and 593 nm emission. PoP was imaged with a filter cube with 400 nm excitation and 679 nm emission. 4 regions of interest were imaged with Dox, PoP, and phase channels. Images were analyzed using the particle analysis function in imageJ after 8-bit conversion and threshold adjustment. The distribution of PoP and Dox was quantified by counting the number of particles.

2.5. Tumor growth inhibition

When tumors reached volumes of 90–200 mm^3, mice were randomized into 4 groups, with 5 mice per group, and were injected via tail vein with: (1) Untreated control; (2) Empty PoP liposomes with laser; (3) LC-Dox-PoP liposomes without laser; (4) LC-Dox-PoP liposomes with laser. Liposomal Dox (4 mg/kg Dox, 0.59 mg/kg PoP) or an equivalent amount of empty PoP liposomes (0.59 mg/kg PoP was administered in 200 μL. Laser irradiation was initiated 1 h post injection for 16.7 min at 200 mW/cm^2 (665 nm, 200 J/cm^2) while mice were anesthetized and placed on a heating pad to maintain body temperature (approx. 35 °C). The entire tumor was irradiated on its surface with a uniform circular laser spot with a 1 mm margin around the tumor. Tumor volumes were calculated using the ellipsoid formula: $Volume = \pi^* L^* \frac{W^2}{6}$, where L and W are the length and width of the tumor. Body weights of the mice were monitored for 3 weeks. Mice were

Table 1
Fitted pharmacokinetics parameters of LC-Dox-PoP liposomes.

Parameter	Definition	Estimate	CV %
CL (mL/h/kg)	Clearance	1.58	2.7
V_p (mL/kg)	Volume of central compartment	42.6	6.2
V_t (mL/kg)	Volume of secondary compartment	11.3	28
Q (mL/h/kg)	Distribution to second compartment	2.15	66
k_1 (1/h/kg)	Drug influx rate to tumor without laser	1.01E-5	11
k_2 (1/h)	Drug efflux rate from tumor without laser	0.0258	16
v_1	CPT-induced influx enhancement factor (applied to k_1)	12.4	18
v_2	CPT-induced efflux enhancement factor (applied to k_2)	3.66	23

CV = Coefficient of variation.

sacrificed when tumor volumes exceeded 10 times the initial volume and never exceeded 2000 mm^3. For immunohistochemistry, mice bearing PDX tumors were injected with 4 mg/kg Dox-PoP liposomes or equivalent empty-PoP liposomes. One hour post injection the mice were treated with a 665 nm laser at a fluence rate of 200 mW/cm^2 for 16.7 min (total fluence 200 J/cm^2). At 48 h post laser treatment the mice were sacrificed, and tumors were surgically removed and placed in formalin. Mouse CD31 staining was conducted by Roswell Park Cancer Institute Histology Facility. Slices were imaged with a 10× objective.

2.6. Pharmacokinetic and pharmacodynamic (PK/PD) analysis

A two-compartment model was used to describe the PK of liposomal Dox. The PK parameters were estimated as shown in Table 1. Equations of the PK model and initial conditions (IC) describing the model are as follows.

The PK of LC-Dox-PoP liposomes in serum was described as:

$$V_p \frac{dC_p}{dt} = -Q \cdot C_p + Q \cdot C_t - Cl \cdot C_p, \quad IC = Dose \tag{1}$$

$$Vt \frac{dC_t}{dt} = Q \cdot C_p - Q \cdot C_t, \quad IC = 0 \tag{2}$$

where Cp and Ct are the concentrations of Dox in serum (central compartment Vp) and tissue (second compartment Vt), CL is clearance from the central compartment, and Q is distribution to second compartment. The PK of liposomal Dox in tumor prior to laser treatment was described as:

$$\frac{dX_{tu}}{dt} = k_1 \cdot X_p - k_2 \cdot X_{tu}, \quad IC = 0 \tag{3}$$

After the tumors were treated with laser, the PK of liposomal Dox in tumor was described as:

$$\frac{dXtu}{dt} = v_1 \cdot k_1 \cdot Xp - v_2 \cdot k_2 \cdot Xtu, \quad IC = 0 \tag{4}$$

where X_{tu} represents the mass of Dox in tumor, k_1 is the influx rate of Dox into tumor without laser, and k_2 is tumor efflux rate without laser treatment, v_1 is the vascular permeabilization factor on the influx rate due to the laser treatment, and v_2 is the vascular permeabilization factor on the tumor efflux rate due to the laser treatment. Laser treatment increases both k_1 and k_2 but to different degrees. The amount of Dox in the tumor is presented rather than the concentration because the tumor volumes were decreased 5 days after treatment. The same approach was reported previously to describe the altered tumor vascular permeability after repetitive administration of sterically stabilized Dox-containing liposomes in a rat brain tumor model [36].

The growth of unperturbed tumor (TV_1) is modeled as exponential growth, where k_{ng} is the first order rate constant of the net tumor growth rate.

$$\frac{dTV_1}{dt} = k_{ng} \cdot TV_1, \; IC = 111 \; mm^3 \tag{5}$$

A nonlinear, direct-effect tumor cell killing model was used to describe the drug-induced tumor shrinkage for both laser-treated and non-laser treated groups [37]. A signal distribution model was used to describe the time delay of the cytotoxic effect of Dox [38]. A nonlinear function of Dox cell kill, which is dependent on the concentration of Dox in the tumor, was used, with $Kmax$ as the maximal cell kill rate and a Michaelis-Menten constant KC_{50}. For the tumors that were treated with LC-Dox-PoP liposomes, tumor volume with/without laser treatment TV_2 was modeled as:

$$\frac{dTV_2}{dt} = kng \cdot TV_2 - K_4 \cdot TV_2, \; IC = 115 \; mm^3 \tag{6}$$

$$\frac{dK_1}{dt} = \frac{1}{\tau} \cdot (K - K_1), \; IC = 0 \tag{7}$$

$$\frac{dK_2}{dt} = \frac{1}{\tau} \cdot (K_1 - K_2), \; IC = 0 \tag{8}$$

$$\frac{dK_3}{dt} = \frac{1}{\tau} \cdot (K_2 - K_3), \; IC = 0 \tag{9}$$

$$\frac{dK_4}{dt} = \frac{1}{\tau} \cdot (K_3 - K_4), \; IC = 0 \tag{10}$$

$$K = \frac{K_{max} \cdot \frac{X_{tu}}{TV_2}}{KC_{50} + \frac{X_{tu}}{TV_2}} \tag{11}$$

Ki represents a series of transit compartments (ie, K_1-K_4). τ is the mean transit time in each transit compartment. There were 4 transit compartments employed with 1 parameter τ.

No tumor growth inhibition was observed for empty-PoP liposomes with laser treatment. Therefore the tumor growth TV_3 for empty PoP liposomes with laser treatment is described as:

$$\frac{dTV_3}{dt} = kpdt \cdot TV_3, \quad IC = 115 \; mm^3 \tag{12}$$

2.7. Data analysis

Differences were considered statistically significant at $p < 0.05$. ADAPT 5 software was used for all data fitting and simulation [39]. The maximum likelihood method was used for fitting the data. Replicate data from animals at each time point in each experiment were naïve-pooled, and serum PK, tumor PK, and tumor growth inhibition for both laser-treated and non-laser treated tumors were fitted sequentially. The goodness of fit was assessed by system convergence, visual inspection of the fitting curves, objective function values such as the Akaike Information Criterion (AIC), improved likelihood, and precision (CV % = S.D./mean*100) of the estimated parameters. The following variance model was used for the model fitting:

$$V_i = V(\theta, \sigma, t) = [(\sigma 1 + \sigma 2 \cdot Y(\theta, t_i)]^2 \tag{13}$$

where $V(\theta, \sigma, t)$ is the variance for the ith point, $Y(\theta, t_i)$ is the ith model-predicted value, θ represents the estimated structural parameters, and $\sigma 1$ and $\sigma 2$ are the variance parameters that were estimated. Non-compartmental analysis was performed in PKsolver [40] with the log linear trapezoidal method.

3. Results

3.1. Enhanced Dox uptake via LC-Dox-PoP liposome chemophototherapy

Laser treatment induced drastic enhancement in Dox deposition. Thirty minutes following laser treatment, there was ~5 fold greater Dox deposition in irradiated tumors compared to non-irradiated ones.

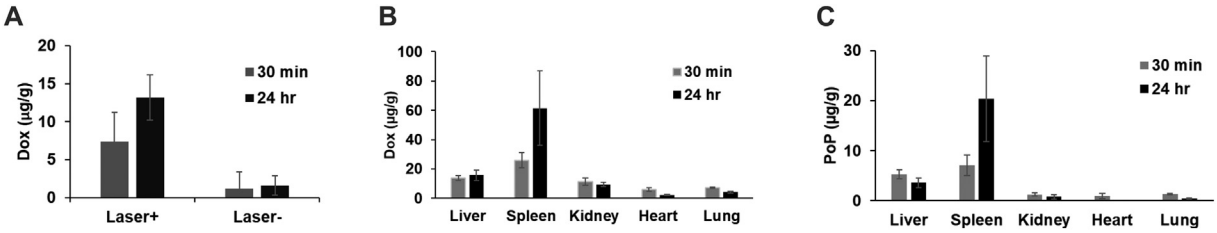

Fig. 1. Enhanced drug uptake by LC-Dox-PoP liposomes following tumor laser treatment. SCID mice bearing dual PDX tumors were administered 7 mg/kg LC-Dox-PoP liposomes intravenously 1 h before laser treatment. (A) Tumor accumulation of Dox was measured 30 min or 24 h after laser treatment (250 mW/cm^2 for 20 min, 300 J/cm^2 Distribution of Dox (B) or PoP (C) in other key organs 30 min or 24 h following administration and laser treatment. Data represent mean ± S.D. for $n = 5$ animals per group.

Twenty-four hr post laser treatment, the drug concentration in the laser-irradiated tumors was nearly 10 fold greater than non-irradiated tumors (Fig. 1A). Dox deposition in key organs was quantified, and the quantity of Dox was high in the spleen and liver, reflecting the removal of circulating nanoparticulates by the reticuloendothelial system (RES) (Fig. 1B). Similar to Dox, PoP liposomes were also mainly deposited in the liver 24 h after drug administration and have very small amount in other organs such as kidney, heart and lung (Fig. 1C). The good agreement of Dox and PoP distribution in key organs suggested that the majority of liposomes were intact with Dox encapsulated.

Unexpectedly, at a dose of 7 mg/kg Dox, SCID mice exhibited substantial body weight loss 12 days after a single intravenous administration, which recovered within a week (Fig. S2A). This likely relates to a pronounced sensitivity of SCID mice to Dox, as this dose is less than half of the maximum tolerated dose for immunocompetent mice [8,41]. No weight loss was observed with LC-Dox-PoP at a 4 mg/kg Dox dose (Fig. S2A), and laser treatment also did not induce weight loss at that dose (Fig. S2B). Because tumor-bearing SCID mice tolerated LC-Dox-PoP liposomes at 4 mg/kg Dox, this dose was used for further investigation.

3.2. PK/PD model

PK/PD modeling approaches were developed to describe quantitatively the enhanced tumor drug delivery process, and a schematic of the final model is shown in Fig. 2. The fitted parameters are shown in Table 1 and Table 2 and discussed below. The Methods section describes the model and associated equations in detail.

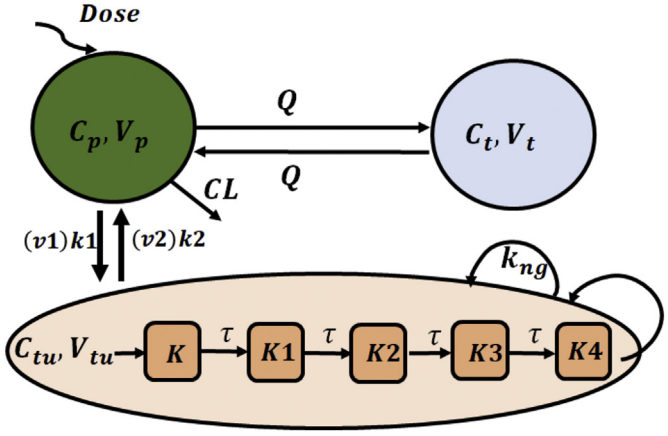

Fig. 2. Pharmacokinetic-Pharmacodynamic (PK/PD) model of LC-Dox-PoP liposomes. *Cp* and *Ct* are the concentrations of Dox in serum (central compartment *Vp*) and tissue (second compartment *Vt*). *CL* is clearance from the central compartment, and *Q* is distribution to second compartment. X_{tu} is the mass of Dox in the tumor. k_1 and k_2 represent the influx and efflux rate of Dox in the tumor without laser treatment. v_1 and v_2 represent the vascular permeabilization factor on the tumor influx and efflux rate, respectively. Laser treatment increases both k_1 and k_2 but to different degrees. See additional symbol definitions in the Methods, Table 1, and Table 2.

Table 2
Fitted pharmacodynamic parameters of LC-Dox-PoP liposomes and CPT response.

Parameter	Definition	Estimate	CV %
KC_{50} ($\mu g/g$)	Dox concentration for 50% tumor cell killing	14.6	35
K_{max} ($1/h$)	Maximum tumor cell killing by Dox	0.978	29
τ (hr)	Mean transit time in each transit compartment	332	11
$k_{ng}(1/h)$	Growth rate of tumor cells	0.00187	2.7
$k_{pdt}(1/h)$	Growth rate of PDT-treated tumor cells	0.00191	2.7

CV = Coefficient of variation.

3.3. Dox blood and tumor kinetics

We assessed Dox kinetics in the tumor and serum of PDX-bearing mice to provide necessary data for the PK/PD analysis. A dose of 4 mg/kg Dox was administered and tumor laser treatment (665 nm laser light, 200 mW/cm^2 for 16.7 min, 200 J/cm^2) was provided using a 1 h drug-light interval (DLI). Laser treatment of the tumor had negligible impact on drug concentrations in blood due to the relatively small blood volume within the tumor vasculature (Fig. S3). A two-compartment model best described the observed serum concentration of LC-Dox-PoP liposomes (Fig. 3A). LC-Dox-PoP liposome PK is characterized by a short α phase and long β phase. Noncompartmental analysis revealed that the PK of liposomal Dox is dose-proportional, with a circulating half-life of 18–19 h and a clearance of ~0.05 mL/h (Table S1).

PoP, which stably embeds in liposomal bilayers, is a photosensitizer, so with laser treatment it can induce PDT effects that permeabilize the tumor vasculature and enhance accumulation of LC-Dox-PoP liposomes. Light-triggered drug release also occurs. The observed data show that Dox tumor concentrations reached a maximum at 4–10 h post laser treatment, and the amount of Dox in laser-treated tumors was up to nearly 11-fold greater than non-laser treated tumors. For a quantitative understanding of the enhanced tumor drug delivery, a tumor drug disposition model was built to analyze the accumulation kinetics of Dox in the tumor, assuming a first-order influx and efflux rates k_1 and k_2. Since the tumor volume is small compared to the total body mass, deposition of Dox in the tumor was assumed to have negligible effect on the serum PK of liposomal Dox. The observed serum PK confirmed the long circulating nature of LC-Dox-PoP in laser-treated mice. The PK/PD model described tumor Dox kinetics well for the tumors that were not irradiated (Fig. 3A). The model also adequately described the Dox tumor deposition profile for the laser-treated tumors, which was fitted by multiplying permeabilization enhancement factors that were applied to the tumor influx and efflux rates. The model estimated that laser treatment increased the influx rate v_1 of Dox by 12.4-fold and increased the efflux rate v_2 by 3.7-fold (Table 1). The estimated ratio of areas under the curve of tumor Dox concentration over time for laser-treated and non-laser treated tumors, $\frac{AUC(laser+)}{AUC(laser+)}$, was 7.0-fold, matching the

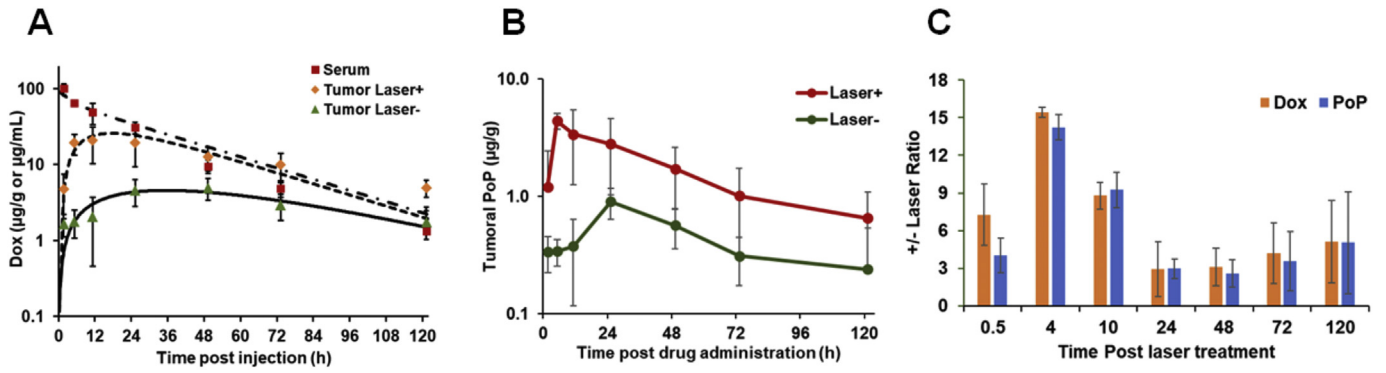

Fig. 3. Observed and modeled Dox serum and tumor kinetics. SCID mice bearing dual PDX tumors were administered LC-Dox-PoP (4 mg/kg) intravenously and 1 h later, only one of the tumors was laser-irradiated (200 mW/cm^2 for 16.7 min, 200 J/cm^2). (A) Observed (symbols) and PK/PD model-predicted profiles (solid or dashed lines) of Dox serum concentration and Dox tumor kinetics with or without tumor laser treatment (in the same animal). (B) Observed PoP concentration kinetics in tumors with or without laser treatment (in the same animal). (C) Ratio of Dox and PoP uptake in tumors with or without laser treatment (in the same animal) at various time post laser treatment. Experimental data represents mean ± S.D. for n = 6 mice per group.

experimental ratio of 7.4 using a linear-up log-down method. At the final time point (120 h), the laser-treated tumors had somewhat greater Dox retention than predicted by the model. A gradual return toward baseline in the treatment-enhanced vascular permeability could result in declining efflux rates and a greater quantity of tumor-retained drug. Although this study did not account for the temporal dynamics of the treatment-mediated vascular permeability changes, the modeling strategy captured the observed data well.

Similar to Dox, PoP concentrations also have significant increase after laser treatment (Fig. 3B), reaching ~14-fold increase 4 h post laser treatment (Fig. 3C). This suggest that the increase of Dox in the tumor is largely due to the increase of intact liposome uptake rather than free Dox. 0.5 after laser treatment, +/− ratio was higher for Dox compared to PoP. The reason for this lower PoP +/− ratio is due to photo bleaching of PoP during laser treatment, as ~30% of photobleaching was seen in vitro after irradiation at 200 mW/cm^2 for 16 min 40 s (Fig. S4). The impact of direct light-triggered release in increasing tumor drug concentration was negligible, as a PDT alone control (empty PoP liposomes plus laser treatment) with Doxil-like liposomes can lead to similar improvement in drug delivery (Fig. S5). Thus, the enhanced tumor drug uptake can be attributed to PDT-induced vascular permeabilization effect. Although light-triggered release didn't directly increase the total drug tumor uptake, leakage of Dox-PoP liposomes after laser treatment will likely increase as in vitro 200 mW/cm^2 light exposure for only 12.5 s would increase the drug leakage to ~45% in 1.5 h while the drug leakage for non-irradiated LC-Dox-PoP is < 1% in 1.5 h (Fig. S6).

3.4. Tumor growth inhibition

Tumor growth inhibition was investigated for a single dose of 4 mg/kg LC-Dox-PoP liposomes in mice bearing a single PDX tumor, using the same drug-light interval and laser irradiation conditions as above. Tumor volume progression in untreated control animals was exponential, with a growth rate of 0.0018/h (Fig. 4A). PDT treatment (empty PoP liposomes with laser treatment) did not inhibit the tumor growth compared to the untreated group (Fig. 4B), and the tumor growth rate was also 0.0018/h. Although PDT itself is a tumor ablation modality, PDT with empty PoP liposomes exerted no anti-tumor efficacy in these PDAC PDX tumors, possibly owing to drug delivery barriers in the tumor model. Drug-loaded LC-Dox-PoP liposomes without laser treatment were somewhat effective in inhibiting the tumor growth, as the tumor volumes were significantly smaller than untreated control group (*p < .05, one-way ANOVA and Tukey' test) on day 52. CPT treatment (LC-Dox-PoP liposomes with laser) also significantly reduced tumor volumes on day 52 compared to untreated control (**p < .05, t-test). There was no significant body weight loss from this treatment (Fig. S2C).

To investigate whether the enhanced efficacy of LC-Dox-PoP liposomes with laser treatment was proportional to the increased Dox accumulation, a PK/PD model was developed to describe treatment-mediated changes in tumor volume progression. A signal transduction model (Fig. 2) was employed to take account of the delayed tumor shrinkage mediated by cytotoxic Dox in both the laser-treated and non-laser treated LC-Dox-PoP liposome groups (Fig. 4C and D). With an assumption in the model that the tumor cell killing effect results only from the cytotoxic effect of tumor-associated Dox, a nonlinear cell killing model estimated a KC_{50} of 14.6 $\mu g/g$ and $Kmax$ of 0.98/h for both the laser-treated and non-laser treated LC-Dox-PoP liposome groups (Fig. 4C and D; Table 2). Thus, this semi-mechanistic PK/PD model can adequately describe the treatment-mediated tumor volume changes for both groups, and suggests that the improved efficacy observed for the LC-Dox-PoP + laser group can be attributed to the enhanced tumor drug accumulation. For the laser treated LC-Dox-PoP liposome group, the model has some overestimation of tumor volumes for the first 13 days (Fig. 4D), possibly due to effects from some released Dox not accounted for by the model. A further limitation of this model is that it does not consider the relationship between free and liposomal doxorubicin, which has recently been assessed in vitro with PK/PD models [42].

3.5. Tumor distribution of LC-Dox-PoP liposomes

Due to its intrinsic fluorescence, Dox can be imaged using fluorescence microscopy of tumor slices. PDX tumor #18269 exhibits stromal amplification and moderately-differentiated pancreatic structures. Without laser treatment, there was limited Dox deposition in tumor (Fig. 5). Laser treatment 1 h after LC-Dox-PoP liposome administration significantly increased the delivery of Dox into the tumor, consistent with the quantification of tumor Dox. Dox and PoP fluorescence exhibited well co-localization. The glandular structures shown the phase micrographs are likely the mucinous vacuoles that typically lined by the adenocarcinoma cells. PoP signal is typically a good indicator of tumor vessels and since Dox pattern is similar to PoP signal, we concluded that LC-Dox-PoP liposomes have limited diffusion from the overlay image.

3.6. Chemophototherapy with longer drug-light intervals

In PDT, the DLI is an important parameter and modulates efficacy and outcomes [43,44]. The PK/PD model described above was used with short DLIs in which vascular permeability enhances drug uptake. Using the developed PK/PD model which is based on simply on

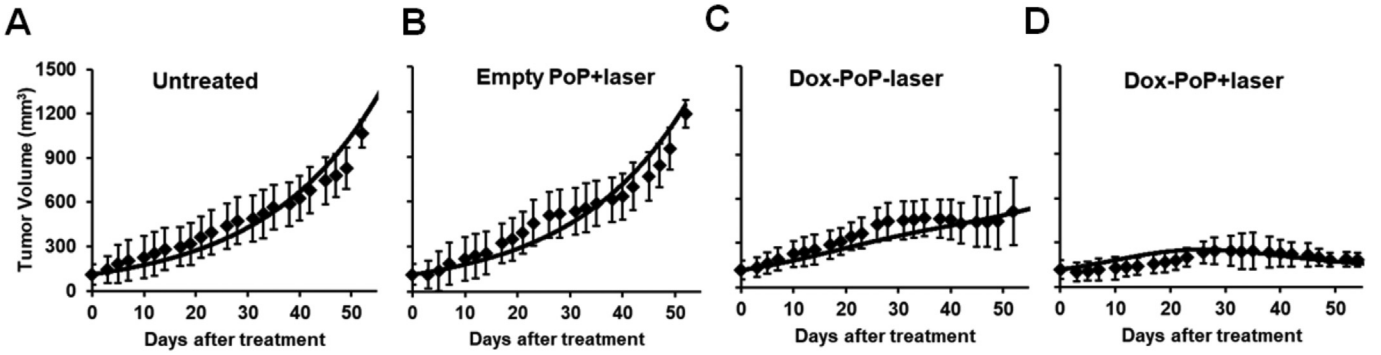

Fig. 4. Observed and modeled tumor growth. Symbols represent observed data and solid lines are the PK/PD model-fitted profiles. (A) Tumor growth in untreated control mice. (B) Tumor growth in mice administered PDT (empty PoP liposomes and treated with laser). Laser treatment was applied 1 h after dosing (0.59 mg/kg PoP). PDT was ineffective under these conditions and the tumor growth rate estimated by the PK/PD model was the same for A and B. (C) Tumor growth in mice given 4 mg/kg LC-Dox-PoP liposomes intravenously but without laser treatment. (D) Tumor growth in mice given 4 mg/kg LC-Dox-PoP liposomes intravenously with laser treatment (200 mW/cm^2 for 16.7 min, 200 J/cm^2) applied 1 h post dosing. Data show mean ± S.D. for $N = 5$ per group.

enhanced vascular permeability, shorter DLIs predict greater tumoral drug uptake (Fig. S7). To investigate the effect of DLI on anti-tumor efficacy, laser irradiation (200 mW/cm^2 for 16.7 min, 200 J/cm^2) was applied at 1, 6, or 24 h post drug administration. Mice treated with a longer DLI appeared to show greater tumor inhibition during the first month. However, no statistical difference in tumor growth occurred (Fig. 6). Thus, additional factors beyond increased drug delivery to the tumor are likely occurring. Further studies with lower Dox doses might be useful to better examine the role of the DLI, since all treatment groups exhibited strong anti-tumor efficacy with these conditions. One explanation was that longer DLIs could enhance efficacy by stronger PDT effects, as more PoP would reside close to the tumor endothelial cells at longer DLI. Tumoral blood flow changes during laser treatment were assessed to gain an insight on the extent of PDT vascular disruption (Fig. 6B). With a 1 h DLI the relative blood flow dropped below 60% of the original blood flow rate immediately after laser application. The blood flow then gradually recovered to ~80% of the initial flow. Laser treatment with a 6 h DLI led to a blood flow decrease to ~40% of the initial blood flow and rebound to ~80% of its initial rate. With a 24 h DLI, tumor blood flow dropped to just 20% of the initial flow and recovered to only ~40% of its initial blood flow. This phenomenon indicates that laser applied at longer DLI (24 h) has a stronger PDT vasculature shutdown effect, reducing blood flow during laser treatment. Additional tumor fluorescence images with 24 h DLI shows greater dispersion of Dox in the tumor (Fig. S8), suggesting an increased portion of Dox released by laser treatment which may contribute to the efficacy of treatment with longer DLI.

Taken together, despite that the simulation results show that a shorter DLI leads to greater drug accumulation of LC-Dox-PoP liposomes, the comparable anti-tumor efficacy of three DLIs at the examined dose may be due to stronger vascular PDT effects and greater amount of intratumoral drug release by laser treatment with longer DLIs. We recently found that in a different xenograft tumor model (MIA PaCa-2), with lower Dox dosing (2 mg/kg) that short DLIs produced stronger anti-tumor effects [45]. That is in contrast to this study in which varying DLIs produced similar anti-tumor efficacy. Although the reason for this discrepancy is unknown, this result underscores the complex mechanisms of CPT, especially when longer DLIs are used.

4. Discussion and conclusions

Pancreatic cancer is characterized by desmoplasia and poor vascularization, which constitute a drug delivery barrier that limits the efficacy of chemotherapy. Therefore, strategies to compromise the drug delivery barrier warrant investigation. The hypovascular PDX tumor model provides an interesting framework to investigate CPT with long-circulating LC-Dox-PoP liposomes. CPT induced a striking increase in Dox accumulation in laser-treated tumors. One caveat of the PDX model is that it necessitates immunocompromised mice, and therefore immune responses induced by the treatment are omitted and combining the treatment with immune checkpoint blockade or other immunotherapies is not possible.

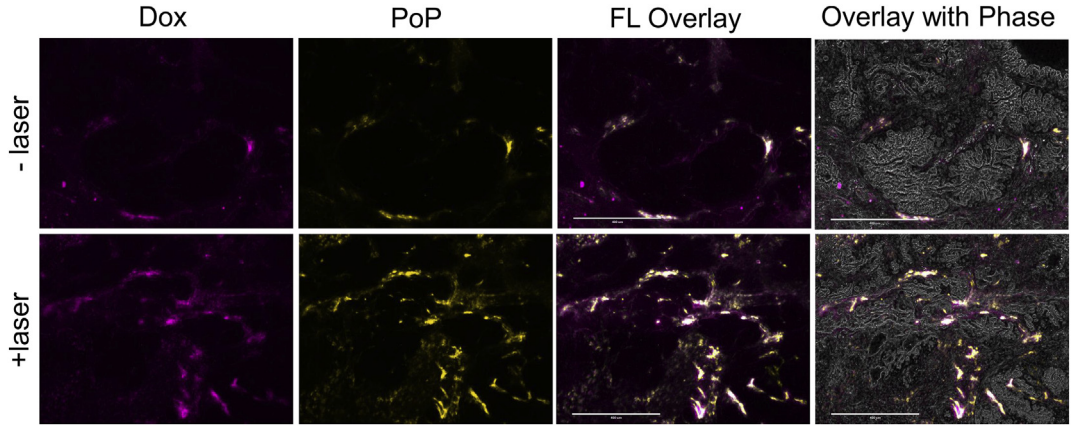

Fig. 5. Fluorescence microscopy of LC-Dox-PoP liposome deposition in tumor slices. Two groups of mice were intravenously administered LC-Dox-PoP liposomes (10 mg/kg Dox). Tumors of one group were laser-irradiated 1 h after liposome administration, using the conditions described (*Methods*), and sacrificed 8 h later. Selected area of tumors were imaged with or without laser treatment. Purple signal indicates Dox, and yellow indicates PoP. Scale bars are 400 μm. (For interpretation of the references to colour in this figure legend, the reader is referred to the web version of this article.)

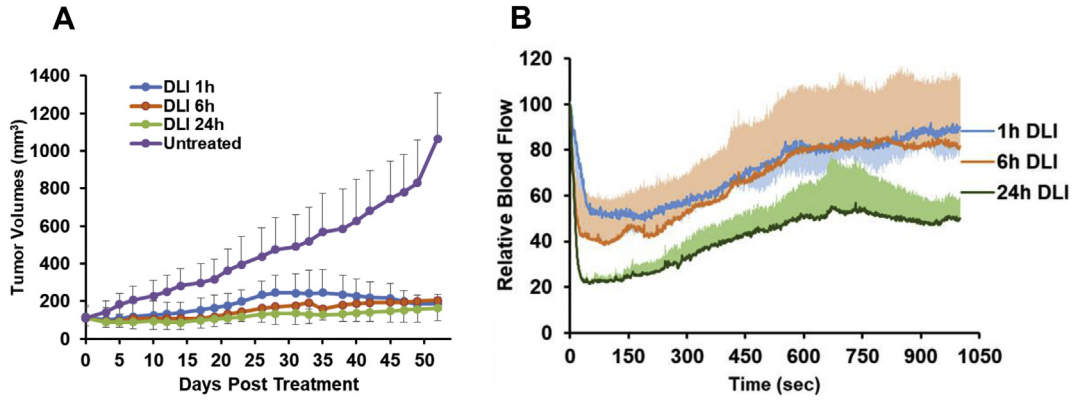

Fig. 6. LC-Dox-PoP liposome efficacy and tumor blood flow during laser treatment with longer DLI. (A) Observed tumor growth in mice treated with various DLIs. LC-Dox-PoP liposomes were administered intravenously (4 mg/kg) and laser treatment (200 mW/cm^2 for 16.7 min, 200 J/cm^2) was applied 1 h, 6 h, or 24 h later. Data show mean ± s.d. for $n = 5$ per group. No statistical difference between each laser treated group was found at any time (One-way ANOVA followed by Tukey's test). (B) Relative moral blood flow during laser treatments shown in B. Laser was initiated at time 0 and ends at 1000s. Data show mean ± s.d. for $N = 3$ per group.

PK/PD modeling was used to provide a quantitative, semi-mechanistic description of LC-Dox-PoP liposome accumulation in tumors following phototreatment. The PK of LC-Dox-PoP liposomes was characterized by a two compartment model, with rapid distribution within the central compartment and slow clearance by the liver and other RES tissues. A tumor drug disposition model with first-order influx and efflux rates were used to describe the deposition of Dox in the tumor. Phototreatment enhanced vascular permeability and the observed Dox kinetics in tumor could largely be accounted for by assuming changes in the influx and efflux rate enhancement factors. To account for tumor growth patterns, the PK/PD model incorporated nonlinear direct cell killing, and a signal transduction model accounted for the delay in drug effects. The model captured the observed data, and suggested that the improved efficacy is directly related to increased tumor drug concentrations (Fig. 4C, D). Additional tumor growth inhibition studies using different Dox doses will be required for more accurate estimation of parameters such as K_{max} and KC_{50} (Table 2). The spatial drug distribution of drug within tumor by fluorescence microscopy further verified the enhanced drug deposition after laser treatment.

To characterize the light treatment regimen further, three different DLI were studied. Simulation with the PK/PD model predicted that shorter DLI would provide greater drug accumulation, assuming that the vascular permeabilization factors were unchanged with different DLI (Fig. S7). Additional studies are required for better understanding of vascular permeabilization and drug deposition processes with different DLIs. At earlier times in the efficacy study with different DLI, tumors treated with the longer DLI showed more pronounced swelling and growth inhibition, suggesting a stronger vascular effect of the PDT component of the mechanism of action. However, the three different DLIs appears to provide similar efficacy at the end of this study.

With a 1 h DLI, no delay in tumor growth was observed with PoP liposomes lacking Dox when laser treatment was applied (Fig. 4B). However, it is known that under appropriate conditions, PDT alone can inhibit tumor growth. There was little liposome deposition in tumors at the early phototreatment time point, especially considering the low perfusion/permeability of the tumor used in this study, which is typical of PDAC [8]. Consequently, a limited PDT effect is not surprising.

It was found that the contribution from intratumor light-triggered release to the total drug increase was negligible and the enhanced tumor drug uptake can be attributed to PDT-induced vascular permeabilization (Fig. S6). Although laser treatment did not directly increase tumor drug disposition, drug leakage for the laser exposed LC-Dox-PoP liposomes will likely increase during the first 2 h after laser treatment (Fig. S7). However, since most drug accumulation occurred after laser treatment, the increased fraction of free drug concentration would be low after 2 h. Our model uses total tumor drug concentration and did not take into account the fraction of drug released 2 h after laser treatment, which is a limitation of this model. With a DLI of 24 h, tumor fluorescence image shows more dispersed microdistribution of Dox signal, suggesting that there may be more free Dox available with 24 h DLI due to light-triggered release (Fig. S8). No difference in tumor vessel microdensity was obviously observed following CPT treatment with a short DLI compared to PDT alone or chemotherapy alone (Fig. S9).

Ongoing human clinical trials of PDT in locally advanced pancreatic cancer have created some optimism for phototherapy [46,47]. However phototherapy and other ablative modalities must avoid damaging critical vessels that are frequently encroached by the tumor in many inoperable patients [48]. Of course, the murine PDX model used in this study was too small to address this and other phototherapy issues such as light penetration depth, which rapidly attenuates in tissue. Fortunately, interstitial fiber optic probes can be inserted into deep and large tumors to facilitate treatment of large tumors [49].

In conclusion, we demonstrated the impact of enhanced vascular permeabilization by laser treatment in increasing the tumor drug accumulation of CPT using LC-Dox-PoP liposomes in a low permeability/perfusion PDAC PDX model. A simple, semi-mechanistic PK/PD model was developed to account quantitatively for observed CPT results. The model estimates that laser treatment induced a ~12 fold increase in the tumor influx rate of LC-Dox-PoP liposomes and a ~4 fold increase in tumor efflux rate, resulting in an overall Dox AUC increase in tumor of 7.4-fold. Further work is required to refine the PK/PD model, test its suitability in other tumor types, and to identify and incorporate additional anti-tumor mechanisms that are more prominent when longer drug-light intervals are used.

Acknowledgements

This work was supported by the National Institutes of Health (R01EB017270, DP5OD017898, R01CA198096, and R01GM024211), the National Science Foundation (1555220), and utilized Roswell Park Cancer Inst. core facilities supported by NIH/NCIP30CA016056. This research was supported in part by a Graduate Student Fellowship Award for DL from the American Association of Pharmaceutical Scientists Foundation. We acknowledge for the assistance of Dr. Prashant K. Singh for assistance in tumor DNA sequencing.

Appendix A. Supplementary data

Supporting information is available online. It includes: DNA sequencing of the KRAS G12D mutation (Fig. S1); mouse body weight after treatment with different doses of LC-Dox-PoP liposomes (Fig. S2);

Pharmacokinetics of LC-Dox-PoP liposomes after laser treatment compared to non-laser treatment (Fig. S3); Photobleaching of PoP and Dox fluorescence during laser treatment (Fig. S4); Enhanced tumor uptake by Doxil-like+ empty PoP liposomes with laser treatment (Fig. S5); Simulation of tumor Dox deposition with 1, 6, or 24 h drug-light intervals (Fig. S6); Dox leakage after laser irradiation (Fig. S7). Fluorescence microscopy of LC-Dox-PoP in tumor slices (Fig. S8). CD31 vessel staining of PDX tumor slices following different treatments (Fig. S9). Non-compartmental analysis of LC-Dox-PoP liposome PK (Table S1). Supplementary data to this article can be found online at https://doi.org/10.1016/j.jconrel.2019.01.030.

References

[1] D. Li, K. Xie, R. Wolff, J.L. Abbruzzese, Pancreatic cancer, Lancet 363 (2004) 1049–1057.
[2] J. Li, M.G. Wientjes, J.L. Au, Pancreatic cancer: pathobiology, treatment options, and drug delivery, AAPS J. 12 (2010) 223–232.
[3] A. Neesse, P. Michl, K.K. Frese, C. Feig, N. Cook, M.A. Jacobetz, M.P. Lolkema, M. Buchholz, K.P. Olive, T.M. Gress, Stromal biology and therapy in pancreatic cancer, Gut 60 (2011) 861–868.
[4] P.P. Provenzano, C. Cuevas, A.E. Chang, V.K. Goel, D.D. Von Hoff, S.R. Hingorani, Enzymatic targeting of the stroma ablates physical barriers to treatment of pancreatic ductal adenocarcinoma, Cancer Cell 21 (2012) 418–429.
[5] A.G. Kohli, S. Kivimäe, M.R. Tiffany, F.C. Szoka, Improving the distribution of Doxil® in the tumor matrix by depletion of tumor hyaluronan, J. Control. Release 191 (2014) 105–114.
[6] L. Eikenes, M. Tari, I. Tufto, Ø.S. Bruland, C. de Lange Davies, Hyaluronidase induces a transcapillary pressure gradient and improves the distribution and uptake of liposomal doxorubicin (Caelyx™) in human osteosarcoma xenografts, Br. J. Cancer 93 (2005) 81.
[7] K.P. Olive, M.A. Jacobetz, C.J. Davidson, A. Gopinathan, D. McIntyre, D. Honess, B. Madhu, M.A. Goldgraben, M.E. Caldwell, D. Allard, K.K. Frese, G. Denicola, C. Feig, C. Combs, S.P. Winter, H. Ireland-Zecchini, S. Reichelt, W.J. Howat, A. Chang, M. Dhara, L. Wang, F. Ruckert, R. Grutzmann, C. Pilarsky, K. Izeradjene, S.R. Hingorani, P. Huang, S.E. Davies, W. Plunkett, M. Egorin, R.H. Hruban, N. Whitebread, K. McGovern, J. Adams, C. Iacobuzio-Donahue, J. Griffiths, D.A. Tuveson, Inhibition of Hedgehog signaling enhances delivery of chemotherapy in a mouse model of pancreatic cancer, Science 324 (2009) 1457–1461.
[8] T. Roy Chaudhuri, N.L. Straubinger, R.F. Pitoniak, B.L. Hylander, E.A. Repasky, W.W. Ma, R.M. Straubinger, Tumor-priming Smoothened inhibitor enhances deposition and efficacy of cytotoxic nanoparticles in a pancreatic cancer model, Mol. Cancer Ther. 15 (2016) 84–93.
[9] A. Gabizon, D. Papahadjopoulos, Liposome formulations with prolonged circulation time in blood and enhanced uptake by tumors, Proc. Natl. Acad. Sci. 85 (1988) 6949–6953.
[10] A. Wang-Gillam, C.-P. Li, G. Bodoky, A. Dean, Y.-S. Shan, G. Jameson, T. Macarulla, K.-H. Lee, D. Cunningham, J.F. Blanc, R.A. Hubner, C.-F. Chiu, G. Schwartsmann, J.T. Siveke, F. Braiteh, V. Moyo, B. Belanger, N. Dhindsa, E. Bayever, D.D. Von Hoff, L.-T. Chen, Nanoliposomal irinotecan with fluorouracil and folinic acid in metastatic pancreatic cancer after previous gemcitabine-based therapy (NAPOLI-1): a global, randomised, open-label, phase 3 trial, Lancet 387 (2016) 545–557.
[11] E. Kipps, K. Young, N. Starling, Liposomal irinotecan in gemcitabine-refractory metastatic pancreatic cancer: efficacy, safety and place in therapy, Ther. Adv. Med. Oncol. 9 (2017) 159–170.
[12] S. Halford, D. Yip, C.S. Karapetis, A.H. Strickland, A. Steger, H.T. Khawaja, P.G. Harper, A phase II study evaluating the tolerability and efficacy of CAELYX (liposomal doxorubicin, Doxil) in the treatment of unresectable pancreatic carcinoma, Ann. Oncol. 12 (2001) 1399–1402.
[13] I. Ahmad, M. Longenecker, J. Samuel, T.M. Allen, Antibody-targeted delivery of doxorubicin entrapped in sterically stabilized liposomes can eradicate lung cancer in mice, Cancer Res. 53 (1993) 1484.
[14] R.E. Eliaz, F.C. Szoka, Liposome-encapsulated doxorubicin targeted to CD44, Cancer Res. 61 (2001) 2592.
[15] X. Guo, F.C. Szoka, Chemical approaches to triggerable lipid vesicles for drug and gene delivery, Acc. Chem. Res. 36 (2003) 335–341.
[16] M.L. Hauck, S.M. LaRue, W.P. Petros, J.M. Poulson, D. Yu, I. Spasojevic, A.F. Pruitt, A. Klein, B. Case, D.E. Thrall, D. Needham, M.W. Dewhirst, Phase I trial of doxorubicin-containing low temperature sensitive liposomes in spontaneous canine tumors, Clin. Cancer Res. 12 (2006) 4004.
[17] D. Luo, K.A. Carter, D. Miranda, J.F. Lovell, Chemophototherapy: an emerging treatment option for solid tumors, Adv. Sci. 4 (2017) 1600106.
[18] P. Agostinis, K. Berg, K.A. Cengel, T.H. Foster, A.W. Girotti, S.O. Gollnick, S.M. Hahn, M.R. Hamblin, A. Juzeniene, D. Kessel, M. Korbelik, J. Moan, P. Mroz, D. Nowis, J. Piette, B.C. Wilson, J. Golab, Photodynamic therapy of cancer: an update, CA Cancer J. Clin. 61 (2011) 250–281.
[19] J.W. Snyder, W.R. Greco, D.A. Bellnier, L. Vaughan, B.W. Henderson, Photodynamic therapy: a means to enhanced drug delivery to tumors, Cancer Res. 63 (2003) 8126–8131.
[20] B. Chen, B.W. Pogue, J.M. Luna, R.L. Hardman, P.J. Hoopes, T. Hasan, Tumor vascular permeabilization by vascular-targeting photosensitization: effects, mechanism, and therapeutic implications, Clin. Cancer Res. 12 (2006) 917–923.
[21] K. Sano, T. Nakajima, P.L. Choyke, H. Kobayashi, Markedly enhanced permeability and retention effects induced by photo-immunotherapy of tumors, ACS Nano 7 (2013) 717–724.
[22] K.A. Carter, S. Shao, M.I. Hoopes, D. Luo, B. Ahsan, V.M. Grigoryants, W. Song, H. Huang, G. Zhang, R.K. Pandey, J. Geng, B.A. Pfeifer, C.P. Scholes, J. Ortega, M. Karttunen, J.F. Lovell, Porphyrin-phospholipid liposomes permeabilized by near-infrared light, Nat. Commun. 5 (2014) 3546.
[23] K.A. Carter, S. Wang, J. Geng, D. Luo, S. Shao, J.F. Lovell, Metal chelation modulates phototherapeutic properties of mitoxantrone-loaded porphyrin–phospholipid liposomes, Mol. Pharm. 13 (2015) 420–427.
[24] K.A. Carter, D. Luo, A. Razi, J. Geng, S. Shao, J. Ortega, J.F. Lovell, Sphingomyelin liposomes containing porphyrin-phospholipid for irinotecan chemophototherapy, Theranostics 6 (2016) 2329.
[25] D. Miranda, K. Carter, D. Luo, S. Shao, J. Geng, C. Li, U. Chitgupi, S.G. Turowski, N. Li, G.E. Atilla-Gokcumen, J.A. Spernyak, J.F. Lovell, Multifunctional liposomes for image-guided intratumoral chemo-phototherapy, Adv. Healthcare Mater. 6 (2017) 1700253.
[26] D. Luo, K.A. Carter, A. Razi, J. Geng, S. Shao, D. Giraldo, U. Sunar, J. Ortega, J.F. Lovell, Doxorubicin encapsulated in stealth liposomes conferred with light-triggered drug release, Biomaterials 75 (2016) 193–202.
[27] G. Song, H. Wu, K. Yoshino, W.C. Zamboni, Factors affecting the pharmacokinetics and pharmacodynamics of liposomal drugs, J. Liposome Res. 22 (2012) 177–192.
[28] M. Tsuchihashi, H. Harashima, H. Kiwada, Development of a pharmacokinetic/pharmacodynamic (PK/PD)-simulation system for doxorubicin in long circulating liposomes in mice using peritoneal P388, J. Control. Release 61 (1999) 9–19.
[29] A. Gasselhuber, M.R. Dreher, F. Rattay, B.J. Wood, D. Haemmerich, Comparison of conventional chemotherapy, stealth liposomes and temperature-sensitive liposomes in a mathematical model, PLoS One 7 (2012) e47453.
[30] M. Hidalgo, F. Amant, A.V. Biankin, E. Budinska, A.T. Byrne, C. Caldas, R.B. Clarke, S. de Jong, J. Jonkers, G.M. Maelandsmo, S. Roman-Roman, J. Seoane, L. Trusolino, A. Villanueva, Patient-derived xenograft models: an emerging platform for translational cancer research, Cancer Discov. 4 (2014) 998–1013.
[31] D. Luo, N. Li, K.A. Carter, C. Lin, J. Geng, S. Shao, W.C. Huang, Y. Qin, G.E. Atilla-Gokcumen, J.F. Lovell, Rapid light-triggered drug release in liposomes containing small amounts of unsaturated and porphyrin-phospholipids, Small 12 (2016) 3039–3047.
[32] G. Haran, R. Cohen, L.K. Bar, Y. Barenholz, Transmembrane ammonium sulfate gradients in liposomes produce efficient and stable entrapment of amphipathic weak bases, Biochim. Biophys. Acta 1151 (1993) 201–215.
[33] B.L. Hylander, R. Pitoniak, R.B. Penetrante, J.F. Gibbs, D. Oktay, J. Cheng, E.A. Repasky, The anti-tumor effect of Apo2L/TRAIL on patient pancreatic adenocarcinomas grown as xenografts in SCID mice, J. Transl. Med. 3 (2005) 22.
[34] G.J. Charrois, T.M. Allen, Drug release rate influences the pharmacokinetics, biodistribution, therapeutic activity, and toxicity of pegylated liposomal doxorubicin formulations in murine breast cancer, Biochim. Biophys. Acta 1663 (2004) 167–177.
[35] K.M. Laginha, S. Verwoert, G.J. Charrois, T.M. Allen, Determination of doxorubicin levels in whole tumor and tumor nuclei in murine breast cancer tumors, Clin. Cancer Res. 11 (2005) 6944–6949.
[36] R.D. Arnold, D.E. Mager, J.E. Slack, R.M. Straubinger, Effect of repetitive administration of Doxorubicin-containing liposomes on plasma pharmacokinetics and drug biodistribution in a rat brain tumor model, Clin. Cancer Res. 11 (2005) 8856–8865.
[37] H. Wong, M. Belvin, S. Herter, K.P. Hoeflich, L.J. Murray, L. Wong, E.F. Choo, Pharmacodynamics of 2-[4-[(1E)-1-(hydroxyimino)-2,3-dihydro-1H-inden-5-yl]-3-(pyridine-4-yl)-1H-pyraz ol-1-yl]ethan-1-ol (GDC-0879), a potent and selective B-Raf kinase inhibitor: understanding relationships between systemic concentrations, phosphorylated mitogen-activated protein kinase kinase 1 inhibition, and efficacy, J. Pharmacol. Exp. Ther. 329 (2009) 360–367.
[38] E.D. Lobo, J.P. Balthasar, Pharmacodynamic modeling of chemotherapeutic effects: application of a transit compartment model to characterize methotrexate effects in vitro, AAPS PharmSci 4 (2002) E42.
[39] D.Z. D'Argenio, A. Schumitzky, X. Wang, ADAPT 5 User's Guide: Pharmacokinetic/Pharmacodynamic Systems Analysis Software, Biomedical Simulations Resource, Los Angeles, 2009.
[40] Y. Zhang, M. Huo, J. Zhou, S. Xie, PKSolver: an add-in program for pharmacokinetic and pharmacodynamic data analysis in Microsoft Excel, Comput. Methods Prog. Biomed. 99 (2010) 306–314.
[41] G.J. Charrois, T.M. Allen, Multiple injections of pegylated liposomal Doxorubicin: pharmacokinetics and therapeutic activity, J. Pharmacol. Exp. Ther. 306 (2003) 1058–1067.
[42] S.K. Soininen, K.-S. Vellonen, A.T. Heikkinen, S. Auriola, V.-P. Ranta, A. Urtti, M. Ruponen, Intracellular PK/PD relationships of free and liposomal doxorubicin: quantitative analyses and PK/PD modeling, Mol. Pharm. 13 (2016) 1358–1365.
[43] R. Veenhuizen, H. Oppelaar, M. Ruevekamp, J. Schellens, O. Dalesio, F. Stewart, Does tumour uptake of Foscan determine PDT efficacy? Int. J. Cancer 73 (1997) 236–239.
[44] M. Triesscheijn, M. Ruevekamp, M. Aalders, P. Baas, F.A. Stewart, Outcome of mTHPC mediated photodynamic therapy is primarily determined by the vascular response, Photochem. Photobiol. 81 (2005) 1161–1167.
[45] D. Luo, K.A. Carter, J. Geng, X. He, J.F. Lovell, Short drug–light intervals improve liposomal chemophototherapy in mice bearing MIA PaCa-2 xenografts, Mol. Pharm. 15 (2018) 3682–3689.
[46] S.G. Bown, A.Z. Rogowska, D.E. Whitelaw, W.R. Lees, L.B. Lovat, P. Ripley, L. Jones, P. Wyld, A. Gillams, A.W.R. Hatfield, Photodynamic therapy for cancer of

the pancreas, Gut 50 (2002) 549–557.
[47] M.T. Huggett, M. Jermyn, A. Gillams, R. Illing, S. Mosse, M. Novelli, E. Kent, S.G. Bown, T. Hasan, B.W. Pogue, S.P. Pereira, Phase I/II study of verteporfin photodynamic therapy in locally advanced pancreatic cancer, Br. J. Cancer 110 (2014) 1698.
[48] S.J.E. Rombouts, J.A. Vogel, H.C.v. Santvoort, K.P.v. Lienden, R.v. Hillegersberg, O.R.C. Busch, M.G.H. Besselink, I.Q. Molenaar, Systematic review of innovative ablative therapies for the treatment of locally advanced pancreatic cancer, Br. J. Surg. 102 (2015) 182–193.
[49] G. Shafirstein, D. Bellnier, E. Oakley, S. Hamilton, M. Potasek, K. Beeson, E. Parilov, Interstitial photodynamic therapy—a focused review, Cancers (Basel) 9 (12) (2017).